

Non-contact Determination of Local Efficiency of mc-Si Solar Cells Using Quantitative Lock-In Thermographic and Carrierographic (Photoluminescence) Imaging

J. Y. Liu · A. Melnikov · A. Mandelis

Received: 29 April 2014 / Accepted: 25 October 2014 / Published online: 7 November 2014
© Springer Science+Business Media New York 2014

Abstract A combined theoretical and experimental approach is developed for determining the local efficiency of multicrystalline silicon solar cells by use of quantitative lock-in carrierographic (LIC, also described as frequency-domain photoluminescence, LIP) and lock-in thermographic (LIT) imaging. The characteristic distribution of the saturation current density J_0 , open-circuit voltage V_{OC} , fill factor FF , and efficiency of solar cell η_s are obtained, and the local inhomogeneities of a solar cell are readily determined by LIT and LIC imaging. The combination of a quantitative LIT and LIC imaging approach is a valuable tool for judging which local defects are especially harmful for degrading the fill factor or the open-circuit voltage.

Keywords Local efficiency · Lock-in carrierographic (photoluminescence) imaging · Lock-in thermographic imaging · Solar cell

List of Symbols

$$A_0 = C_{LIT} J_0, A_g = C_{LIT} J_g, \\ C = \frac{\hbar\omega_{in}}{q\eta\eta_{cc}(\hbar\omega, 0, T)} \quad \text{Intermediate parameters}$$

J. Y. Liu (✉)
School of Mechatronics Engineering, Harbin Institute of Technology,
Harbin 150001, Heilongjiang, People's Republic of China
e-mail: ljywlj@hit.edu.cn

J. Y. Liu · A. Melnikov · A. Mandelis
Center for Advanced Diffusion Wave Technologies (CADIFT), Mechanical and
Industrial Engineering, University of Toronto, Toronto, ON M5S 3G8, Canada

A. Mandelis
e-mail: mandelis@mie.utoronto.ca

$C_{\text{LIT}}, C_{\text{LIC}}$	Calibration factor of LIT and LIC
$F_{\text{R}}(V, T)$	Radiative-recombination emission photon flux
$F_{\text{i}}(\hbar\omega)$	Incident photon flux
$F_{\text{ce}}[\hbar\omega, V(\hbar\omega), T]$	Photocarrier flux collected at the p – n junction
FF	Fill factor
$ \text{LIT}[V(\omega_{\text{M}})] _{x,y}$,	LIT amplitude and LIC amplitude distribution
$ \text{LIC}[V(\omega_{\text{M}})] _{x,y}$	
$J_{\text{g}}, J_{\text{D}}, J_0$	Photogenerated current density, injection current density, and saturation diode current density
$J[\hbar\omega, V(\hbar\omega), T]_{\text{R}}$	Nonequilibrium radiative recombination current density
$J_{\text{R}} = q \cdot \eta \eta_{\text{R}}(\hbar\omega, V_{\text{OC}}, T)$	Relevant current-like quantities
$F_{\text{i}}(\hbar\omega), J_{\text{R}0} = q F_{\text{R}}(0, T)$	
$ I_{\text{i}} $	
R	Surface reflectance
S	Illuminated surface area of the solar cell
V_{OC}	Open-circuit voltage
$Z(\hbar\omega) = Z(\hbar\omega) \cdot e^{i\phi(\hbar\omega)} \cdot e^{i\omega_{\text{M}}t}$	Complex quantities
n, n_j	Ideality factor of solar cell and optoelectronic ideality factor
$\alpha(E)$	Absorptivity of an emitter of non-thermal radiation
η, η_{ce}	Quantum efficiency and photocarrier-to-collection current efficiency
η_{s}	Efficiency of solar cell
$\hbar\omega_{\text{in}}, \hbar\omega_{\text{em}}$	Incident and mean radiative-recombination-emission photon energy
$\eta_{\text{NR}}, \eta_{\text{R}}$	Quantum efficiency for non-radiative and radiative recombination
$\lambda_{\text{in}}, \lambda_{\text{em}}$	Photon wavelengths corresponding to $\hbar\omega_{\text{in}}$ and $\hbar\omega_{\text{em}}$

1 Introduction

The current–voltage characteristic plays an important role in estimating the performance of solar cells. It directly determines the quality and conversion efficiency. The current–voltage characteristic can be described by the electrical fundamental parameters of the solar cell. Over the past two to three decades, many infrared radiometric methods have been used to evaluate the performance of solar cells. They mainly include photothermal radiometry (PTR), lock-in thermography (LIT), photoluminescence imaging (PL), photocarrier radiometry (PCR), and lock-in carrierography (LIC), among others [1–5].

Lock-in thermography (LIT), which includes dark lock-in thermography (DLIT) and illumination lock-in thermography (ILIT), is a useful characterization imaging technique widely used in solar cell research [6–9]. LIT is available for detection of

shunts, series resistance, and grain boundaries, and can be used to determine the power loss based on an appropriate calibration.

Long-pass-filtered dynamic lock-in photoluminescence imaging (LIPI), also known as lock-in carrierography (LIC) imaging, was recently developed [10] as the dynamic imaging extension of photocarrier radiometry (PCR) [11]. It has the advantage of filtering out the thermal infrared (non-radiative) component of the emission spectrum of de-exciting free photocarriers, and/or resolving the radiative versus the non-radiative components through spectrally windowed modulation frequency scans, thereby being sensitive only to radiative recombination events when performing dynamic measurements of transport properties in semiconductors [12].

In this paper, the relation between the LIT amplitude, power loss flux, and a quantitative calibration expression for the LIT amplitude is described. A quantitative relation [14, 15] that links the radiative recombination emission flux to the electrical parameters of solar cells is used for the determination of the same fundamental parameters by means of LIC measurements. Furthermore, both LIT and LIC are used to determine the local efficiency of a solar cell.

2 Experimental Apparatus and Procedures

2.1 Samples

An industrial multicrystalline-Si (mc-Si) solar cell ($156 \times 156 \text{ mm}^2$, 0.2 mm thickness) from Enfoton Solar Ltd., Cyprus, was used for both LIT and LIC measurements.

2.2 Description of Experimental Technique

2.2.1 Principle of the Technique

Non-thermal radiation, as encountered in semiconductors under nonequilibrium conditions, has been described with the generalization of Planck's law as introduced by Würfel [13]. For optoelectronic semiconductor materials of bandgap energy $E > 1 \text{ eV}$, and small photovoltages such that $E - qV \ll k_B T$, where q is the elementary charge and $k_B T$ is the thermal energy, the emitted photon flux can be accurately simplified as

$$F_R(V, T) \cong \left[\left(\frac{\alpha(E)(E)^3}{4\pi^2 \hbar^3 c^2} \right) \exp\left(\frac{-E}{k_B T}\right) \right] \exp\left(\frac{qV}{k_B T}\right). \quad (1)$$

$\eta_{ce}[\hbar\omega, V(\hbar\omega), T]_{x,y}$ is defined to be the carrier collection efficiency, the ratio of the collected carrier flux to the photogenerated carrier flux [14–16],

$$\eta_{ce}[\hbar\omega, V(\hbar\omega), T]_{x,y} = \frac{F_{ce}[\hbar\omega, V(\hbar\omega), T]_{x,y}}{\eta F_i(\hbar\omega)}. \quad (2)$$

Quantum efficiencies for non-radiative and radiative recombination, η_{NR} and η_R , are given at open-circuit [14–16] conditions,

$$\eta_{NR}(V_{OC}, T)_{x,y} = \frac{\eta_{ce}(\hbar\omega, 0, T)_{x,y} - \lambda_{in}\lambda_{em}^{-1}}{1 - \lambda_{in}\lambda_{em}^{-1}}, \tag{3a}$$

$$\eta_R(V_{OC}, T)_{x,y} = \frac{1 - \eta_{ce}(\hbar\omega, 0, T)_{x,y}}{1 - \lambda_{in}\lambda_{em}^{-1}}. \tag{3b}$$

The photogenerated current density (bias voltage $V(\hbar\omega) = 0$) is given by [14]

$$J_g(x, y) = qF_{ce}[\hbar\omega, 0, T]_{x,y} = q\eta\eta_{ce}(\hbar\omega, 0, T)_{x,y}F_i(\hbar\omega). \tag{4}$$

The dissipated power flux E_{loss} of a solar cell under monochromatic illumination is related to the photogenerated current density J_g , the injection current density J_D , the photovoltage $V(\hbar\omega)$, and the photon energy $\hbar\omega_{in}$ [1–4]:

$$E_{loss}(x, y) = V(\hbar\omega) [J_D(x, y) - J_g(x, y)] + \hbar\omega_{in}F_i(\hbar\omega). \tag{5}$$

Furthermore, the injection current density depends exponentially on the photovoltage,

$$J_D(x, y) = J_0(x, y) \left\{ \exp \left[\frac{qV(\hbar\omega)}{n(x, y)k_B T} \right] - 1 \right\}. \tag{6}$$

It should be noted that for dynamic imaging modalities at an angular modulation frequency ω_M , such as in LIT and LIC imaging, complex quantities are implied with the general form, $Z(\hbar\omega) = |Z(\hbar\omega)| \cdot e^{i\phi(\hbar\omega)} \cdot e^{i\omega_M t}$. The LIT amplitude is proportional to the dissipated power, and the proportionality factor can be identified as a calibration factor, C_{LIT} [3],

$$|LIT[V(\omega_M)]|_{x,y} = C_{LIT}(x, y)E_{loss}(x, y). \tag{7}$$

The calibration factor, C_{LIT} , is given by [14]

$$C_{LIT}(x, y) = \frac{|LIT[V_{OC}(\omega_M)]|_{x,y}}{|I_i|(1 - R)} \frac{1 - \lambda_{in}\lambda_{em}^{-1}}{\eta_{ce}(\hbar\omega, 0, T)_{x,y} - \lambda_{in}\lambda_{em}^{-1}}. \tag{8}$$

From Eqs. 5 and 7, an expression for the LIT amplitude related to the electrical parameters of the solar cell can be derived as

$$|LIT[V(\omega_M)]|_{x,y} = A_0 V(\omega_M) \left[\exp \left(\frac{qV(\omega_M)}{nk_B T} \right) - 1 \right] + A_g [C - V(\omega_M)], \tag{9}$$

where $A_0 = C_{LIT}(x, y)J_0(x, y)$, $A_g = C_{LIT}(x, y)J_g(x, y)$, and $C = \frac{\hbar\omega_{in}}{q\eta\eta_{ce}[\hbar\omega, 0, T]_{x,y}}$.

From Eq. 9, the electrical fundamental parameters of a solar cell can be accurately estimated by means of LIT measurements.

In LIC, the influence of the excess minority carrier reabsorption is negligible [10], as the absorption efficiency for radiatively emitted luminescence photons is small. Introduction of an optoelectronic ideality factor n_j describing radiative recombination

processes, an equation has been derived that is only related to the nonequilibrium radiative recombination process [14, 15],

$$F_R[\hbar\omega, V(\omega_M), T]_{x,y} = C_{LIC}(x, y) |LIC[V(\omega_M)]|_{x,y}, \tag{10a}$$

$$J[\hbar\omega, V(\hbar\omega), T]_R = J_R(x, y) - J_{R0}(x, y) \left\{ \exp \left[\frac{qV(\hbar\omega)}{n_j(x, y)k_B T} \right] - 1 \right\}, \tag{10b}$$

where $J_R(x, y) = q \cdot F_R(\hbar\omega, V_{OC}, T)_{x,y}$ and $J_{R0}(x, y) = q F_R(0, T)_{x,y}$.

The calibration factor and photogenerated current density are given by [14, 15]

$$C_{LIC}(x, y) = \frac{\eta |I_1| (1 - R)}{\hbar\omega_{in} \cdot J_R(x, y)} \frac{1 - \eta_{ce}(\hbar\omega, 0, T)_{x,y}}{1 - \lambda_{in}\lambda_{em}^{-1}} \tag{11}$$

and

$$J_g(x, y) = q C_{LIC}(x, y) J_R(x, y) \left[\frac{(1 - \lambda_{in}\lambda_{em}^{-1})}{(\eta_{ce}(\hbar\omega, 0, T)_{x,y}^{-1} - 1)} \right] \tag{12a}$$

$$J_0(x, y) = q C_{LIC}(x, y) J_{R0}(x, y). \tag{12b}$$

A number of expressions can be derived. The most relevant quantities are the open-circuit photovoltage relationship,

$$V_{OC}(x, y) \approx n(x, y) \frac{k_B T}{q} \ln \left[\frac{J_g(x, y)}{J_0(x, y)} \right] = n_j(x, y) \frac{k_B T}{q} \ln \frac{J_R(x, y)}{J_{R0}(x, y)} \tag{13}$$

and an expression for the fill factor (*FF*) has been provided by Ghosh et al. [17],

$$FF(x, y) \approx \left\{ 1 - \frac{1}{\ln \left[\frac{J_g(x, y)}{J_0(x, y)} \right]} \right\} = 1 - \frac{1}{\ln \left(\frac{J_R(x, y)}{J_{R0}(x, y)} \frac{1 - \lambda_{in}\lambda_{em}^{-1}}{\eta_{ce}(\hbar\omega, 0, T)_{x,y}^{-1} - 1} \right)}. \tag{14}$$

The solar cell efficiency is obtained from

$$\eta_s(x, y) = \frac{J_g(x, y) V_{OC}(x, y) FF(x, y)}{|I_1|}. \tag{15}$$

2.2.2 Apparatus

For the LIT and LIC measurement setup made as shown in Fig. 1a, the optical-to-photocarrier flux can be described according to Fig. 1b. A mid-infrared camera (Cedip Titanium 550 from FLIR) with a 320 × 256 pixel active element, spectral bandwidth of 2.5 μm to 5.0 μm, and frame rate of 150 Hz for a full window size was used for LIT measurements. A near-infrared camera (SU320KTSW-1, 7RT/RS170 from Goodrich Sensors Unlimited) with a long-pass filter (~1000 nm) was used for LIC measurements. This camera has a 320 × 256 pixel active element, spectral bandwidth

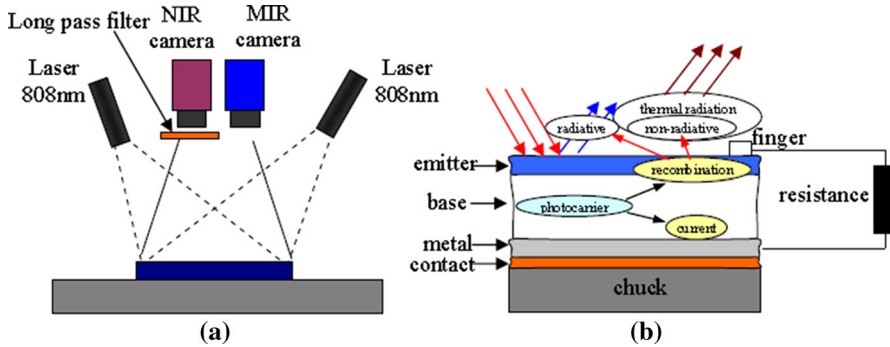


Fig. 1 (a) LIT and LIC measurement setup and (b) optical-to-photocarrier conversion channels

of $0.9\ \mu\text{m}$ to $1.7\ \mu\text{m}$, frame rate of 119.6 Hz for full window size, and full-frame exposure times ranging from 0.13 ms to 16.6 ms. The solar cell was illuminated from the front side using a superband-gap fiber coupled 16 W/808 nm diode laser. The laser beam was spread and homogenized by engineered microlens arrays forming a square illumination area with a uniform intensity. A data acquisition module from National Instruments was used to generate the modulation waveform for the laser current. The modulation frequency was set at 10 Hz, and the LIC and LIT amplitude and phase images were produced using in-house developed software.

A series of load resistances were used to measure the I - V characteristics of our solar cell with dc illumination provided by the same 808 nm diode laser under the same conditions. The current I through the load resistance R_L and the photovoltage V across R_L were obtained from electrical measurements (EM).

3 Results

The LIT and LIC experiments were carried out in two different experimental systems, and the light intensity was set as close as possible to $0.04\ \text{W}\cdot\text{cm}^{-2}$. In practice, the illumination intensity was measured to be $0.043\ \text{W}\cdot\text{cm}^{-2}$ and $0.038\ \text{W}\cdot\text{cm}^{-2}$ for the LIT and LIC measurements, respectively. The I - V characteristic, power output versus photovoltage curve and their theoretical best fits to the solar cell diode equation without a series resistance are shown in Fig. 2. The photovoltage corresponding to maximum power, $V_{p\text{max}} = 0.462\ \text{V}$ ($I_i = 0.043\ \text{W}\cdot\text{cm}^{-2}$) and $V_{p\text{max}} = 0.460\ \text{V}$ ($I_i = 0.038\ \text{W}\cdot\text{cm}^{-2}$) was obtained from the peak of the fitted curve in Fig. 2b. The fill factor and solar efficiency were calculated using $FF = P_{\text{max}}/V_{\text{oc}}J_{\text{sc}}S$ and $\eta_s = P_{\text{max}}/I_i \cdot S$, respectively. $FF = 72.14\%$, $\eta_s = 18.3\%$ ($I_i = 0.043\ \text{W}\cdot\text{cm}^{-2}$) and $FF = 72.24\%$, $\eta = 18.6\%$ ($I_i = 0.038\ \text{W}\cdot\text{cm}^{-2}$) were also obtained from Fig. 2. Therefore, it indicates that the electrical performance (FF and η_s) of the solar cell is fully similar for two different light intensities.

To validate the proportionality between the LIT amplitude and power dissipation, the voltage-dependent LIT measurements are shown in Fig. 3. The calibration factor based on non-radiative recombination according to Eq. 8 was used to calibrate the LIT amplitude image dependence on power losses. The total power dissipated in the

Fig. 2 (a) I - V characteristics and (b) output power curve dependence on photovoltage; illumination power density: $0.043 \text{ W}\cdot\text{cm}^{-2}$ and $0.038 \text{ W}\cdot\text{cm}^{-2}$

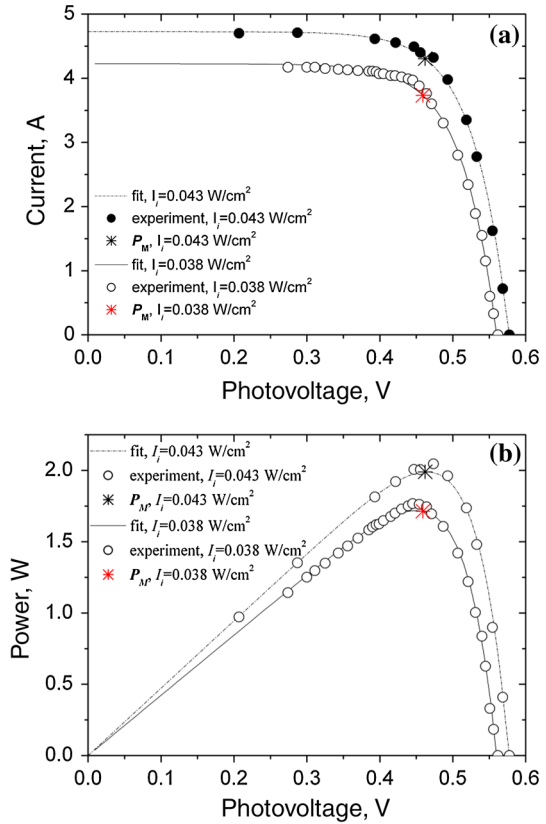
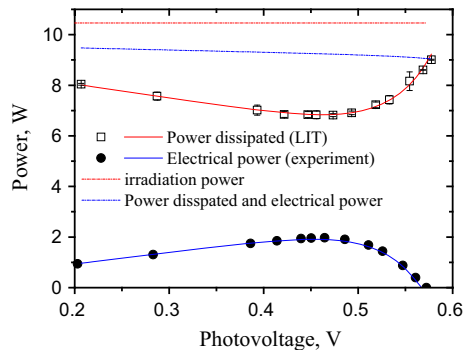


Fig. 3 LIT solar cell power measurement; illumination power density: $0.043 \text{ W}\cdot\text{cm}^{-2}$; modulation frequency: 10 Hz



whole solar cell for every voltage setting was determined from the LIT measurements by integration over the entire solar cell area. By adding the electrically extracted power to the dissipated power measured by LIT, we obtained a variable power component over the entire voltage range as seen in Fig. 3. This power component is less than the irradiation power incident into the cell. This indicates that a small fraction of the irradiation power is reflected by the solar cell surface as well as emitted by pho-

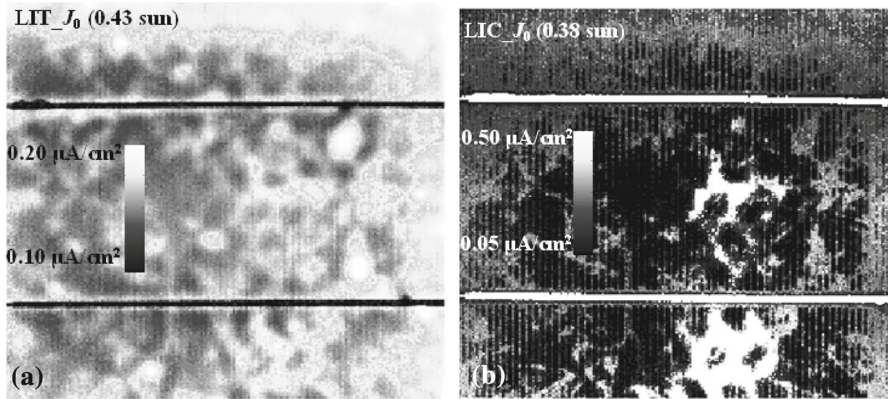


Fig. 4 Saturation diode current density J_0 images using LIT and LIC imaging at 10Hz: (a) LIT- J_0 image and (b) LIC- J_0 image. All scaling ranges are indicated; *scaling bars* in (a) hold for both images

to carrier radiative recombination after absorption. The LIT-calculated photovoltage corresponding to maximum power $V_{pmax} = 0.464$ V was obtained at the minimum value of the dissipated power in Fig. 3.

Figure 4 shows saturation diode current density J_0 images of the solar cell calculated as derivative images from LIT and LIC images. The J_0 images, scaled in $\mu\text{A}\cdot\text{cm}^{-2}$, are shown in Fig. 4a and b using the LIT and LIC images, respectively. From the LIT image, Fig. 4a, the local saturation diode current density J_0 of the solar cell is seen to vary between $0.1 \mu\text{A}\cdot\text{cm}^{-2}$ to $0.2 \mu\text{A}\cdot\text{cm}^{-2}$, and local inhomogeneities are apparent with high contrast. From the LIC image, Fig. 4b, the local saturation diode density, J_0 , of the solar cell is seen to vary between $0.05 \mu\text{A}\cdot\text{cm}^{-2}$ to $0.5 \mu\text{A}\cdot\text{cm}^{-2}$, and local inhomogeneities are also apparent with high contrast. The images agree with the theoretical expectation that a high local concentration of recombination centers crossing the $p-n$ junction leads to pronounced enhanced recombination which is responsible for the high saturation diode current density and/or high ideality factors [8].

In Fig. 5 various local cell parameters are shown using LIT and LIC imaging, which are obtained assuming full illumination intensity ($I_i = 0.043 \text{ W}\cdot\text{cm}^{-2}$ for LIT imaging; and $I_i = 0.038 \text{ W}\cdot\text{cm}^{-2}$ for LIC imaging). It is seen that the LIT V_{OC} at $0.043 \text{ W}\cdot\text{cm}^{-2}$ and the LIC V_{OC} at $0.038 \text{ W}\cdot\text{cm}^{-2}$ (from Fig. 5a and d, respectively) are mainly influenced by local maxima of the saturation diode current density (in Fig. 4). The opposite holds for the FF distributions in Fig. 5b and e, respectively, which are more strongly influenced by the maxima of the saturation diode current density. All local efficiency variations (Fig. 5c and f, respectively) may be explained by variations of V_{OC} or FF . The local solar cell efficiency analysis using LIT and LIC measurements is consistent with earlier results [8]. From Figs. 4 and 5, the saturation diode current density, J_0 , and the FF of the LIC measurements exhibit a higher dynamic range than the respective LIT measurements. It can be seen that the LIC measurements are more sensitive to local inhomogeneities than the LIT measurements, and the LIC-derived V_{OC} , FF , and η images show high spatial resolution and contrast.

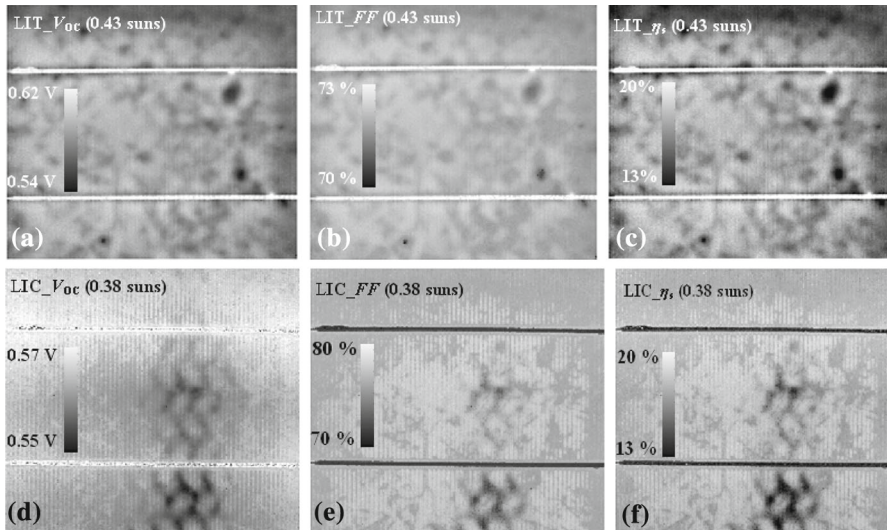


Fig. 5 (a) LIT- V_{OC} at $0.043 \text{ W}\cdot\text{cm}^{-2}$, (b) LIT- FF at $0.043 \text{ W}\cdot\text{cm}^{-2}$, (c) LIT- η_s at $0.043 \text{ W}\cdot\text{cm}^{-2}$, (d) LIC- V_{OC} at $0.038 \text{ W}\cdot\text{cm}^{-2}$, (e) LIC- FF at $0.038 \text{ W}\cdot\text{cm}^{-2}$, and (f) LIC- η_s at $0.038 \text{ W}\cdot\text{cm}^{-2}$. All scaling ranges are indicated and *scaling bars* in (d) hold for all images

4 Conclusions

We have demonstrated that quantitative LIT and LIC imaging can be used to analyze the local inhomogeneities and local efficiencies of solar cells. LIC has the advantage of higher spatial resolution and contrast, including the saturation diode current density J_0 , open-circuit voltage V_{OC} , fill factor FF , and efficiency η_s images. The combination of quantitative LIT and LIP imaging can be a more valuable tool for judging which local defects are especially harmful for degrading the fill factor or the open-circuit voltage than either technique alone.

Acknowledgments A. Mandelis is grateful to NSERC for a Discovery grant, to the Canada Foundation for Innovation (CFI) for equipment grants, to the Canada Research Chairs Program, and to the Ontario Ministry for Research and Innovation (MRI) for the Inaugural Premier's Discovery Award in Science and Technology (2007).

References

1. D. Cahen, B. Büchner, P. Decker, M. Wolf, IEEE Trans. Electron Dev. **37**, 498 (1990)
2. H. Flaisher, M. Wolf, D. Cahen, J. Appl. Phys. **66**, 1832 (1989)
3. M. Wolf, D. Cahen, Solar Cells **27**, 247 (1989)
4. D. Cahen, Appl. Phys. Lett. **33**, 810 (1978)
5. A. Mandelis, J. Appl. Phys. **66**, 5572 (1989)
6. O. Breitenstein, M. Langenkamp, M.H.A. Rifai, Prog. Photovolt. Res. Appl. **11**, 515 (2003)
7. O. Breitenstein, M. Langenkamp, O. Lang, A. Schirmacher, Sol. Energy Mater. Sol. Cells **65**, 55 (2001)
8. O. Breitenstein, Sol. Energy Mater. Sol. Cells **107**, 381 (2012)
9. O. Breitenstein, J.P. Rakotoniaina, J. Appl. Phys. **97**, 074905 (2005)

10. A. Melnikov, A. Mandelis, J. Tolev, P. Chen, S. Huq, J. Appl. Phys. **107**, 114513 (2010)
11. A. Mandelis, J. Batista, D. Shaughnessy, Phys. Rev. B **67**, 205208 (2003)
12. A. Melnikov, A. Mandelis, J. Tolev, E. Lioudakis, J. Phys. Conf. Ser. **214**, 012111 (2010)
13. P. Würfel, J. Phys. C **15**, 3967 (1982)
14. J.Y. Liu, A. Melnikov, A. Mandelis, Phys. Status Solidi A **210**, 2135 (2013)
15. J.Y. Liu, A. Melnikov, A. Mandelis, J. Appl. Phys. **114**, 104509 (2013)
16. A. Mandelis, Y. Zhang, A. Melnikov, J. Appl. Phys. **112**, 054505 (2012)
17. A.K. Ghosh, C. Fishman, T. Teng, J. Appl. Phys. **51**, 446 (1980)